

Note and calculations concerning elastic dilatancy in 2D glass-glass liquid foams

François Molino, Pierre Rognon, and Cyprien Gay*

Centre de Recherche Paul Pascal, CNRS, UPR 8641,
 Université de Bordeaux 1, 115 Av. Schweitzer, F-33600 PESSAC, France
 Department of Endocrinology, Institute of Functional Genomics, CNRS,
 UMR 5203, INSERM U661, Universities of Montpellier 1 and 2,
 141 rue de la Cardonille, F-34094 MONTPELLIER cedex 05, France
 Matière et Systèmes Complexes, Université Paris Diderot-Paris 7, CNRS, UMR 7057,
 Bâtiment Condorcet, Case courrier 7056, F-75205 PARIS cedex 13, France
 (Dated: February 15, 2022)

When deformed, liquid foams tend to raise their liquid contents like immersed granular materials, a phenomenon called dilatancy. We have already described a geometrical interpretation of elastic dilatancy in 3D foams and in very dry foams squeezed between two solid plates (2D GG foams). Here, we complement this work in the regime of less dry 2D GG foams. In particular, we highlight the relatively strong dilatancy effects expected in the regime where we have predicted rapid Plateau border variations.

PACS numbers: 47.20.Dr, 83.80.Iz, 47.57.Bc, 68.03.Cd

I. DILATANCY IN FOAMS

Liquid foams [1, 2] and granular materials both exhibit “dilatancy”, described by Reynolds [3] in the context of granular materials: upon deformation, because grains are forced to move while avoiding each other, the medium swells to some extent. In other words, the fluid volume fraction ϕ is increased (see Fig. 1). This effect can remain unnoticed in air. By contrast, a spectacular absorption of liquid [4] is obtained upon deformation of an immersed granular sample.

Because bubbles can deform individually, a foam might

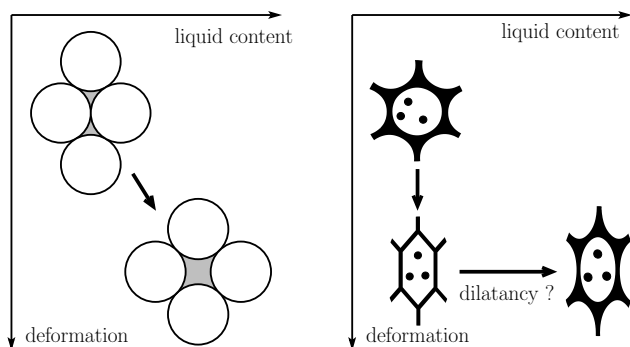


FIG. 1: Dilatancy in granular media and in foams. When a granular material (left), initially in a compact state, is deformed, the steric interactions between grains cause the liquid content to rise. By contrast, in a foam (right), because the bubbles are deformable, the liquid volume fraction may remain constant. Static dilatancy means that if the liquid fraction tends to increase due to the applied deformation.

deform substantially without altering its liquid fraction (see Fig. 1). Hence, there is *a priori* no reason why a foam should display dilatancy. In fact, dilatancy *does exist* in foams. This has been shown both experimentally [5] in the case of “dynamic” dilatancy (caused by a continuous foam deformation) and theoretically [6–8] in the case of “elastic” dilatancy (caused by a constant deformation of the foam).

Dilatancy can be defined [6] in terms of the osmotic pressure of a foam confined in a container, which corresponds to the force that must be applied externally to one of the confining walls if the latter is permeable to the liquid but not to the bubbles. The static dilatancy coefficient χ reflects the fact that the foam osmotic pressure varies with the deformation ϵ when the fluid volume fraction ϕ is kept constant:

$$\chi = \left. \frac{\partial^2 \pi_{\text{osm}}}{\partial \epsilon^2} \right|_{\phi} \quad (1)$$

Surprisingly, this coefficient can be either *positive* like in granular materials or *negative* [6]. In the case of a negative dilatancy coefficient, deforming the foam results in a tendency to expell liquid and make the foam dryer.

We have shown that the origin of this change in sign can be traced back to two different physical contributions [8]. On the one hand, deforming the foam implies an increase in the total of all Plateau border lengths in the sample (in the case of a 2D GG foam [9], these are the *pseudo* Plateau borders, *i.e.*, those along the solid plates). As a result of this increase in length, when the total amount of liquid is kept constant, the Plateau borders shrink, which raises the pressure difference between the gas and the liquid, resulting in an increase of the osmotic pressure, hence a positive contribution to dilatancy. On the other hand, deforming the foam also implies an increase in the total surface area of the gas-liquid interfaces. Because the interfaces contribute negatively to the stress tensor in the foam (tensile contribution),

*Electronic address: cyprien.gay@univ-paris-diderot.fr

this has a negative contribution to the osmotic pressure, and hence, to dilatancy. Because the increase in total interfacial energy is directly related to the elasticity of the foam, this negative contribution to dilatancy coefficient is proportional to the elastic modulus, as shown by Weaire and Hutzler [6],

In the present work, with this geometrical interpretation in mind, we conduct the explicit calculation of the elastic dilatancy of not too dry 2D GG foams (regimes A, B, C and D). In particular, we highlight the relatively strong dilatancy effects expected in the regime where we have predicted rapid Plateau border variations.

II. GEOMETRY OF 2D GG FOAMS: FLOOR TILE VERSUS PANCAKE REGIME

Let us first choose notations [8, 10] to describe the geometry of two-dimensional foams squeezed between two glass plates, called “GG” foams.

We call L the perimeter of the bubble, defined as the perimeter of the rounded polygon that constitutes the bubble, as seen from above, and R the corresponding radius of curvature of the Plateau border (see Fig. 2, left). We call H the distance between both solid plates, and R_{ps} the radius of curvature of the pseudo Plateau borders (see Fig. 2, bottom right). We also call Ω the average bubble volume, and Ω_{liq} the average volume of liquid per bubble. The liquid volume fraction ϕ thus verifies:

$$\phi = \frac{\Omega_{liq}}{\Omega + \Omega_{liq}}, \quad i.e. \quad \Omega_{liq} = \Omega \frac{\phi}{1 - \phi}. \quad (2)$$

We assume that Ω remains constant: the applied stresses are not sufficient to compress the gas phase significantly unless the bubble size is on the order of a micron.

The main contributions to the quantity of liquid per bubble are pictured on Fig. 2 and can be calculated from simple geometrical arguments:

$$\Omega_{liq} \simeq (2 - \pi/2) L R_{ps}^2 + (2\sqrt{3} - \pi) R^2 H \quad (3)$$

The first term corresponds to the pseudo Plateau borders, which make the junction between the interbubble films and the solid plates. As seen from above, they correspond to the light grey regions in Fig. 2. Each portion of their interfaces has the shape of a quarter of a circular cylinder (see Fig. 2, bottom right). The second term in Eq. (3) corresponds to the genuine Plateau borders (black regions in Fig. 2), whose three contours span an angle $\pi/3$ each.

Eq. (3) indicates that the squeezed 2D foam can be found in two main regimes depending on volume fraction and geometry. They are pictured on Fig. 3.

1. When the Plateau border radius R is much larger than the sample thickness H (regimes A-D of Fig. 3), each bubble takes the form of a thick “pancake”, and its edge is like a half cylinder with radius $H/2$.

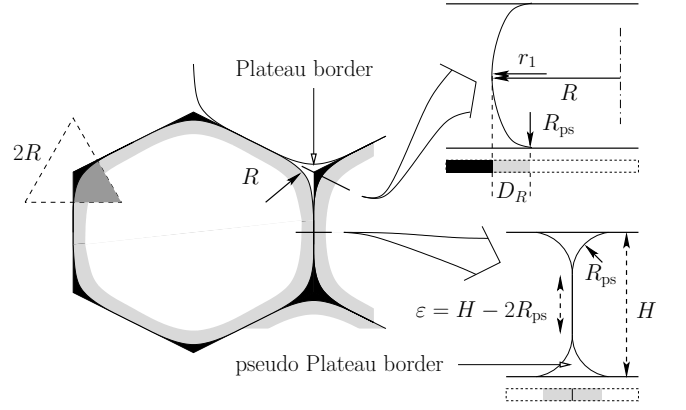


FIG. 2: Pancake conformation of a bubble squeezed between two solid plates (distance H): approximate geometry. Left: top view. The variable L denotes the average perimeter of the bubbles in such a top view (outer perimeter of the light grey region). The variable Ω is the volume of the bubble gas (full thickness of the white region and part of the thickness of the light grey region), and \mathcal{A} is defined as $\mathcal{A} = \Omega/H$. The variable \mathcal{A}_{tot} is the total (gas and liquid) projected surface area per bubble (white and light grey and black regions). The Plateau rules imply that the angle of the medium grey sector is $\pi/3$. Right: two different cross-sections (side views) with matching greyscale. As seen from above, the contact between two bubbles is typically along a straight line (left). The pseudo Plateau borders then have a uniform curvature in this region (radius R_{ps} , see bottom right drawing). By contrast, in the Plateau border region, the section of the gas-liquid interface is approximately elliptical in shape (top right drawing), with radii of curvature r_1 at mid-height in the vertical direction and R_{ps} at the plates, while the radius of curvature at mid-height in the horizontal direction is R . The width D_R of the curved region is intermediate between R_{ps} and $H/2$ while r_1 is larger than $H/2$.

$\phi < \phi_c$	$R < L$	A	$R^3 > L^2 H$	-
-	$R^3 < L^2 H$	B	$R^2 > L H$	$\Omega_{Pb} > \Omega_{pPb}$
$\Omega_{Pb} < \Omega_{pPb}$	$R^2 < L H$	C	$R^3 > L H^2$	-
-	$R^3 < L H^2$	D	$R > H$	pancake
floor tile	$R < H$	E	$L > H$	2D
stretched 2D	$L < H$	F	$L^2 > H R$	-
-	$L^2 < H R$	G	$L > R$	$\phi < \phi_c$

TABLE I: Seven regimes for a 2D glass-glass foam. Regimes A-D correspond to pancake-shaped bubbles, while regime E corresponds to a foam made of floor tile shaped bubbles. In regimes C-E, most of the liquid is located in the pseudo Plateau borders, whereas in regime A and B, the Plateau borders themselves have a greater volume. The transitions between regimes A and B, and that between C and D (which are meaningful as far as dilatancy is concerned) have no simple geometrical interpretation. Note that regimes F and G, where the height is larger than the perimeter, do not always correspond to stable 2D GG foams, as shown in Ref. [11]. But the limit $H \rightarrow \infty$ in regime G corresponds to an ideal 2D foam.

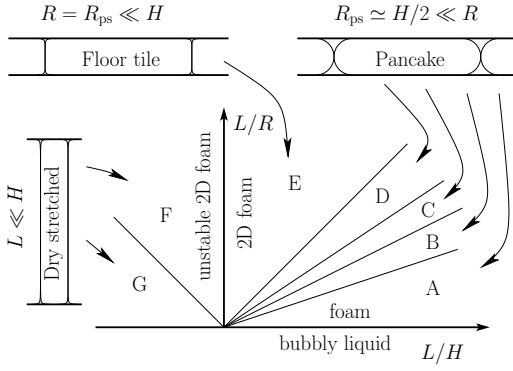


FIG. 3: Regimes of a glass-glass 2D foam with low liquid fraction foam ($\phi \ll 1$), in terms of the bubble perimeter L , the Plateau border radius R and the cell height H . The bubble perimeter L is measured at mid-height of the cell: it is the outer perimeter of the light grey ribbon in Fig. 2. Such a foam can be found in two main configurations. In the floor tile situation (regimes E-G) the pseudo Plateau borders are much thinner than the cell height ($R = R_{ps} \ll H$). By contrast, in the pancake regime, although the overall liquid volume fraction ϕ is still much smaller than 1, facing pseudo Plateau borders almost join ($H - 2R_{ps} \ll H \ll R$), and each bubble has a pancake-like shape. More precisely, when considering properties such as dilatancy, it is useful to subdivide the pancake situation into regimes A-D defined by Table I. The corresponding expressions for the liquid volume fraction and for dilatancy are indicated on Tables II and III. Note that regimes F and G, where the height is larger than the perimeter, do not always correspond to stable 2D GG foams, as shown in Ref. [11]. The limit of a truly two-dimensional foam is obtained in regime G with $H \rightarrow \infty$.

2. In the reverse limit, the bubbles are shaped more like “floor tile”, with sharp edges (regime E of Fig. 3): this time, the Plateau borders are like fine threads pinned on both solid plates, and each pseudo Plateau borders resembles a stretched, fine thread, glued on one of the solid plate and joining the attachment points of two Plateau borders.

In Fig. 3, we have also pictured regimes F and G: they are useful to obtain the limit of ideal 2D foams, for which the solid plates are so far apart that the volume of the pseudo Plateau borders can be entirely neglected. Regime G is useful in particular for dilatancy [8] as it reproduces the negative dilatancy result obtained in the very dry limit [6]. Note that as shown by Cox, Weaire and Vaz both analytically and numerically [11], any bubbles with less than six neighbours will tend to gather on one of the solid plates for large separations, thus turning the foam into a three-dimensional rather than two-dimensional foam. As a result, in the case where all bubbles inside the foam have exactly six or more (hence exactly six) neighbours, the plates can be separated indefinitely without triggering any rearrangements.

In the pancake regime (A-D), one has $R_{ps} \simeq H/2$.

Taking into account the elliptical shape of the Plateau border cross-section taken perpendicularly to the plates (see Ref. [10] for details), the volume of liquid per bubble can be expressed as:

$$\Omega_{\text{liq}}^{\text{ABCD}} \simeq \frac{4 - \pi}{8} H^2 L \left[1 - \frac{2H}{3R} \right] + (2\sqrt{3} - \pi) R^2 H \quad (4)$$

In regimes A and B, the Plateau border contribution dominates: $\Omega_{\text{liq}} \simeq (2\sqrt{3} - \pi) R^2 H$. Conversely, in regimes C and D, the pseudo Plateau borders contain most of the liquid: $\Omega_{\text{liq}} \simeq (1/2 - \pi/8) L H^2$.

In all three regimes E-G ($R \ll H$, floor tile regime), the radius of curvature R_{ps} of the pseudo Plateau borders is equal to that of the Plateau borders $R_{ps}^{\text{EFG}} = R$ and Eq. (3) reduces to:

$$\Omega_{\text{liq}}^{\text{EFG}} \simeq [(2 - \pi/2) L + (2\sqrt{3} - \pi) H] R^2 \quad (5)$$

III. DILATANCY IN THE CD REGIME

In this Section, we focus on regimes C and D, see Fig.3 They are defined by the following conditions:

$R^2 < LH$	C	$R^3 > LH^2$
$R^3 < LH^2$	D	$R > H$

Indeed, we have shown that in these regimes, the size of the Plateau borders change in a particularly rapid manner [10] as a function of volume fraction ϕ , inter-plate distance H or bubble size L . We thus expect stronger dilatancy effects in these two regimes. We will demonstrate below that it is indeed the case.

In order to conduct the corresponding calculation, our first aim is to obtain an expression relating the variation $\delta\phi$ of the liquid volume fraction, the variation $\delta\pi_{\text{osm}}$ of the osmotic pressure and the variation δL of the perimeter (related to the foam deformation ϵ).

We start from

$$\phi^{CD} \simeq \frac{4 - \pi}{8} \frac{H^2 L}{\Omega} \quad (6)$$

$$\begin{aligned} \pi_{zz}^{CD} &\simeq \frac{2\gamma}{H} \\ \pi_{pl}^{CD} &\simeq \frac{2\gamma}{3R} \end{aligned} \quad (7)$$

which are obtained (in regimes C and D) from Eqs. (A3) and (C24-C25).

Differentiating Eqs. (A3) and (C24-C25), we obtain:

$$\delta\phi^C = \frac{4 - \pi}{8} \frac{H^2}{\Omega} \delta L + (4\sqrt{3} - 2\pi) \frac{RH}{\Omega} \delta R, \quad (8)$$

$$\delta\phi^D = \frac{4 - \pi}{8} \frac{H^2}{\Omega} \delta L + \frac{4 - \pi}{12} \frac{H^3 L}{\Omega R^2} \delta R, \quad (9)$$

$$\begin{aligned}\delta\pi_{zz} + \frac{2\gamma}{H}\delta\phi &= -\frac{2}{3}\frac{\gamma}{R^2}\delta R - \frac{\pi}{4}\frac{\gamma H}{\Omega}\delta L, \\ \delta\pi_{pl} + \frac{2\gamma}{R}\delta\phi &= -\frac{2}{3}\frac{\gamma}{R^2}\delta R - \frac{\pi}{8}\frac{\gamma H}{\Omega}\delta L.\end{aligned}\quad (10)$$

Eliminating δR between the equations for $\delta\phi$ and $\delta\phi$, we obtain:

$$\delta\pi_{zz,pl}^C + \frac{2}{3(4\sqrt{3}-2\pi)}\frac{\gamma\Omega}{R^3H}\delta\phi = \frac{4-\pi}{12(4\sqrt{3}-2\pi)}\frac{\gamma H}{R^3}\delta L, \quad (11)$$

$$\delta\pi_{zz,pl}^D = -\frac{8}{4-\pi}\frac{\gamma\Omega}{H^3L}\delta\phi + \frac{\gamma}{HL}\delta L. \quad (12)$$

As shown in Ref. [8], the variation of the perimeter is related to the foam deformation in the following way, see Appendix B:

$$\frac{\delta L}{L} = \frac{\epsilon^2}{2} \quad (13)$$

Then, using

$$\Omega = L^2H, \quad (14)$$

$$\frac{LH^2}{\Omega} = \frac{H}{L} \ll 1, \quad (15)$$

and

$$\frac{LHR}{\Omega} = \frac{R}{L} \ll 1, \quad (16)$$

we get:

$$\delta\pi_{zz,pl}^C + \frac{2}{3(4\sqrt{3}-2\pi)}\frac{\gamma\Omega}{R^3H}\delta\phi = \frac{4-\pi}{24(4\sqrt{3}-2\pi)}\frac{\gamma HL}{R^3}\epsilon^2 \quad (17)$$

$$\delta\pi_{zz,pl}^D + \frac{8}{4-\pi}\frac{\gamma\Omega}{H^3L}\delta\phi = \frac{1}{2}\frac{\gamma}{H}\epsilon^2 \quad (18)$$

Setting $\delta\phi = 0$, we obtain the dilatancy coefficients defined by Eq. (1), which characterize the immediate change in osmotic pressure due to the foam deformation:

$$\chi^C = \frac{4-\pi}{12(4\sqrt{3}-2\pi)}\frac{\gamma HL}{R^3}, \quad (19)$$

$$\chi^D = \frac{\gamma}{H}. \quad (20)$$

Conversely, setting $\delta\pi = 0$, we obtain the eventual change in liquid fraction that results from a deformation ϵ :

$$\delta\phi^{CD} = \frac{4-\pi}{16}\frac{H^2L}{\Omega}\epsilon^2. \quad (21)$$

Using

$$\phi^C = \phi^D = \frac{4-\pi}{8}\frac{H^2L}{\Omega}, \quad (22)$$

we get the relative change in liquide volume fraction:

$$\frac{\delta\phi}{\phi} = \frac{1}{2}\epsilon^2 = \frac{\delta L}{L}. \quad (23)$$

Quantity	Eqs.	Value	Regimes
pseudo Plateau border radius	R_{ps} Ref. [10]	$\frac{H}{2} \left(1 - \frac{H}{3R}\right)$ R	ABCD EFG
volume of liquid per bubble	Ω_{liq} (4, 5)	$(2\sqrt{3}-\pi)R^2H$ $\frac{4-\pi}{8}LH^2$ $\frac{4-\pi}{2}LR^2$	ABFG CD E
liquid volume fraction ($\phi = \frac{\Omega_{liq}}{\mathcal{A}_{tot}H}$)	ϕ (A1-A4)	$(2\sqrt{3}-\pi)\frac{R^2}{\mathcal{A}_{tot}}$ $\frac{4-\pi}{8}\frac{LH}{\mathcal{A}_{tot}}$ $\frac{4-\pi}{2}\frac{R^2L}{\mathcal{A}_{tot}}$	ABFG CD E
specific surface area	Σ Ref. [10]	$\frac{2}{H} - \frac{(4\sqrt{3}-2\pi)R^2}{\mathcal{A}_{tot}H}$ $\frac{2}{H} + \frac{\pi-2}{2}\frac{L}{\mathcal{A}_{tot}}$ $\frac{2}{H} + \frac{L}{\mathcal{A}_{tot}}$ $\frac{L}{\mathcal{A}_{tot}}$	AB CD E FG
normal osmotic pressure (C24, C26)	π_{osm}^{zz}	$2\frac{\gamma}{H} + \frac{2}{3}\frac{\gamma}{R} - \frac{\pi}{4}\frac{\gamma LH}{\Omega}$ $\frac{\gamma}{R} - \frac{\gamma LH}{\Omega}$	ABCD EFG
in-plane osmotic pressure (C25, C27)	π_{osm}^{pl}	$\frac{2}{3}\frac{\gamma}{R} - \frac{\pi}{8}\frac{\gamma LH}{\Omega}$ $\frac{\gamma}{R} - 2\frac{\gamma}{H} - \frac{1}{2}\frac{\gamma LH}{\Omega}$	ABCD EFG
shear modulus (D17-D18)	G	$\frac{\pi}{16}\frac{\gamma LH}{\Omega}$ $\frac{1}{4}\frac{\gamma LH}{\Omega}$	ABCD EFG

TABLE II: Geometrical and stress properties of a two-dimensional glass-glass foam. The numbers refer to the relevant series of equations and the letters to the regimes of Fig. 3: pancake regime (A-D) and floor tile regime (E-G).

IV. CONCLUSION

In the present follow-up to References [8, 10], we derived detailed mechanical properties of two-dimensional foams squeezed between parallel solid surfaces.

The main geometrical and mechanical properties of such foams are summarized in Tables II and III and in the corresponding equations indicated therein.

After recalling our geometrical interpretation of elastic dilatancy in very dry 2D GG and 3D foams [8], we derived the expected magnitude of such effects for less dry 2D GG foams.

It must be recalled, at this stage, that the calculations were carried out in some asymptotic limits defined by Table I. Some of these regimes (particularly A-D) are rather narrow: for comparison with a real situation, it will be more advisable to use the full equations cited in Table III than each asymptotic expression listed within the table. To get more accurate results, in particular in regimes C and D, Surface Evolver simulations would be required as in Refs. [10, 12].

Concerning dilatancy, the main result of our calculations is that the expected effect is positive in most regimes (B-F): deforming the foam will induce an *increase* in the osmotic pressure if the volume is kept constant, or conversely it will induce an *increase* in the liquid volume fraction if the osmotic pressure is kept constant. Only regimes A and G display negative dilatancy [6]: in these regimes, among both contributions to the osmotic

Quantity	Eqs.	Value	Regimes
Plateau border variation	$\left. \frac{\delta R/R}{\delta L/L} \right _\phi$ (D8, D10)	$-\frac{4-\pi}{32\sqrt{3}-16\pi} \frac{LH}{R^2}$ $-\frac{3}{2} \frac{R}{H}$ $-\frac{1}{2}$ $-\frac{4-\pi}{8\sqrt{3}-4\pi} \frac{L}{H}$	ABC D E FG
Normal elongational dilatancy χ_{zz}^{el}	$\left. \frac{\delta \pi_{\text{osm}}^{zz}}{\delta L/L} \right _\phi$ (D23, D25)	$-\frac{\pi}{4} \frac{\gamma L H}{\Omega} = -4 G^{\text{ABCD}}$ $\frac{4-\pi}{12(4\sqrt{3}-2\pi)} \frac{\gamma H L}{R^3}$ $\frac{\gamma}{H}$ $\frac{1}{2} \frac{\gamma}{R}$ $\frac{4-\pi}{8\sqrt{3}-4\pi} \frac{\gamma L}{R H}$ $-\frac{\gamma H P}{\Omega} = -4 G^{\text{EFG}}$	A BC D E F G
In-plane elongational dilatancy χ_{pl}^{el}	$\left. \frac{\delta \pi_{\text{osm}}^{pl}}{\delta L/L} \right _\phi$ (D24, D26)	$-\frac{\pi}{8} \frac{\gamma L H}{\Omega} = -2 G^{\text{ABCD}}$ $\frac{4-\pi}{12(4\sqrt{3}-2\pi)} \frac{\gamma H L}{R^3}$ $\frac{\gamma}{H}$ $\frac{1}{2} \frac{\gamma}{R}$ $\frac{4-\pi}{8\sqrt{3}-4\pi} \frac{\gamma L}{R H}$ $-\frac{1}{2} \frac{\gamma H L}{\Omega} = -2 G^{\text{EFG}}$	A BC D E F G
Liq. fraction variation at constant normal π_{osm}^{zz}	$\left. \frac{\delta \phi/\phi}{\delta L/L} \right _{\pi_{\text{osm}}^{zz}}$ (D38, D40)	$-\frac{\pi}{4(4\sqrt{3}-2\pi)} \frac{LH}{R^2}$ $\frac{4-\pi}{4(4\sqrt{3}-2\pi)} \frac{LH}{R^2}$ 1 $\frac{4-\pi}{4\sqrt{3}-2\pi} \frac{L}{H}$ $-2 \frac{LH R}{\Omega}$	A B CDE F G
Liq. fraction variation at constant in-plane π_{osm}^{pl}	$\left. \frac{\delta \phi/\phi}{\delta L/L} \right _{\pi_{\text{osm}}^{pl}}$ (D39, D41)	$-\frac{3\pi}{8} \frac{LH R}{\Omega}$ $\frac{4-\pi}{4(4\sqrt{3}-2\pi)} \frac{LH}{R^2}$ 1 $\frac{4-\pi}{4\sqrt{3}-2\pi} \frac{L}{H}$ $-\frac{LH R}{\Omega}$	A B CDE F G

TABLE III: Predictions for dilatancy. The variation of the Plateau border radius is taken at constant volume fraction. The elongational dilatancy coefficient is related to the shear coefficient through Eq. (D33). For both the variation of the liquid fraction at constant osmotic pressure and the elongational dilatancy coefficient, the normal mode as well as the in-plane mode are provided. The numbers refer to the relevant series of equations and the letters to the regimes of Fig. 3.

pressure discussed in Ref. [8] and recalled in the Introduction, the effect of the increase in total surface area dominates over the effect of the increase in total pseudo Plateau border length.

As we mentioned in the Introduction, the Plateau borders vary rapidly in size in regimes C and D [10]. Let us now discuss how that affects dilatancy.

As can be seen in Table III, the relative change in volume fraction at constant in-plane osmotic pressure π_{osm}^{pl} , divided by the square of the deformation, $\epsilon^2 = 2\delta L/L$ (see Appendix B), is of order unity in regimes C, D and E. It can be checked, using Table I, that the same quantity is much smaller in neighbouring asymptotic regimes

B and F. The same observation holds at constant normal osmotic pressure π_{osm}^{zz} .

Regarding both the in-plane and the normal dilatancy coefficients χ_{pl}^{el} and χ_{zz}^{el} , the same is true. Indeed, taking their expressions in regime E as a reference, $\chi^{\text{el}}(E) \simeq \gamma/R$, one can check, again using Table I, that they become bigger in regimes C and D and smaller in B and F.

We believe that regimes S and D should therefore *a priori* constitute the more promising target for experimental investigations.

Acknowledgements

We gratefully acknowledge fruitful discussions with Benjamin Dollet and with participants of the GDR 2352 Mousses (CNRS) and of the Informal Workshop on Foam mechanics (Grenoble 2008). P.R. was supported by the Agence Nationale de la Recherche (ANR05).

Appendix A: Liquid volume fraction

From Eqs. (4) and (5), we derive the liquid volume fraction $\phi = \Omega_{\text{liq}}/(\mathcal{A}_{\text{tot}} H)$ in the foam, both in the pancake regime and in the floor tile regime:

$$\phi^{\text{ABCD}} \simeq \frac{4-\pi}{8} \frac{H L}{\mathcal{A}_{\text{tot}}} \left[1 - \frac{2H}{3R} \right] + (2\sqrt{3}-\pi) \frac{R^2}{\mathcal{A}_{\text{tot}}} \quad (\text{A1})$$

$$\phi^{\text{EFG}} \simeq \frac{4-\pi}{2} \frac{R^2 L}{\mathcal{A}_{\text{tot}} H} + (2\sqrt{3}-\pi) \frac{R^2}{\mathcal{A}_{\text{tot}}} \quad (\text{A2})$$

The corresponding values of ϕ in all sub-regimes are indicated in Table II. Because the total volume of the bubble and liquid, $\mathcal{A}_{\text{tot}} H = \Omega + \Omega_{\text{liq}}$, is not constant, it is useful to express the liquid fraction in terms of the volume Ω of the bubble itself. Using $\phi/(1-\phi) = \mathcal{A}_{\text{tot}} H \phi/\Omega$, the above equations become:

$$\frac{\phi^{\text{ABCD}}}{1-\phi^{\text{ABCD}}} \simeq \frac{4-\pi}{8} \frac{H^2 L}{\Omega} \left[1 - \frac{2H}{3R} \right] + (2\sqrt{3}-\pi) \frac{R^2 H}{\Omega} \quad (\text{A3})$$

$$\frac{\phi^{\text{EFG}}}{1-\phi^{\text{EFG}}} \simeq \frac{4-\pi}{2} \frac{R^2 L}{\Omega} + (2\sqrt{3}-\pi) \frac{R^2 H}{\Omega} \quad (\text{A4})$$

Appendix B: Bubble perimeter in a crystalline 2D foam

Let us consider a crystalline foam subjected to an arbitrary elastic, homogeneous deformation. Up to a global

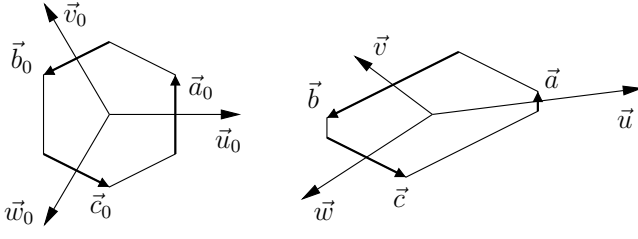


FIG. 4: One hexagonal bubble in a crystalline, two-dimensional foam at rest (left) and after deformation (right). Center-to-center vectors \vec{u}_0 , \vec{v}_0 and \vec{w}_0 are transported affinely according to the macroscopic deformation, see Eqs. (B7-B9). By contrast, bubble edges (vectors \vec{a}_0 , \vec{b}_0 and \vec{c}_0) rearrange after deformation (vectors \vec{a} , \vec{b} and \vec{c}), in order to meet at angle $2\pi/3$.

rotation, it can be expressed as an elongation:

$$\begin{pmatrix} \lambda & 0 \\ 0 & 1/\lambda \end{pmatrix} \quad (\text{B1})$$

The perimeter of such a hexagonal foam increases upon deformation in the following way [16] :

$$L^{\text{dry}} = L_0^{\text{dry}} \left[\frac{\lambda}{2} + \frac{1}{2\lambda} \right] \quad (\text{B2})$$

$$\frac{\delta L}{L_0^{\text{dry}}} = \frac{(\lambda - 1)^2}{2\lambda} \quad (\text{B3})$$

To show it, we consider a crystalline, two-dimensional foam in the dry limit, and derive the total interface contour length in the foam as a function of the applied deformation.

Let us start with an undeformed foam. The initial bubble edges \vec{a}_0 , \vec{b}_0 and \vec{c}_0 meet at angle $2\pi/3$ according to Plateau's rule, and they have identical lengths (hence, $\vec{a}_0 + \vec{b}_0 + \vec{c}_0 = \vec{0}$), see Fig. 4a. The center-to-center vectors

$$\vec{u}_0 = \vec{c}_0 - \vec{b}_0 \quad (\text{B4})$$

$$\vec{v}_0 = \vec{a}_0 - \vec{c}_0 \quad (\text{B5})$$

$$\vec{w}_0 = \vec{b}_0 - \vec{a}_0, \quad (\text{B6})$$

which coincide with the principal crystalline axes, then also meet at angle $2\pi/3$. When the foam is deformed (transformation F), these vectors are deformed according to:

$$\vec{u} = F \cdot \vec{u}_0 \quad (\text{B7})$$

$$\vec{v} = F \cdot \vec{v}_0 \quad (\text{B8})$$

$$\vec{w} = F \cdot \vec{w}_0 \quad (\text{B9})$$

Correspondingly, the bubble edges \vec{a} , \vec{b} and \vec{c} reorganize so as to not only verify

$$\vec{u} = \vec{c} - \vec{b} \quad (\text{B10})$$

$$\vec{v} = \vec{a} - \vec{c} \quad (\text{B11})$$

$$\vec{w} = \vec{b} - \vec{a}, \quad (\text{B12})$$

but also maintain the $2\pi/3$ angle condition. This generally implies evolving towards unequal lengths (see Fig. 4b).

For simplicity, we restrict ourselves to a deformation that conserves the bubble volume (*i.e.*, surface area as seen from above):

$$\begin{aligned} S &= \frac{\sqrt{3}}{2} (a_0 b_0 + b_0 c_0 + c_0 a_0) = \frac{3\sqrt{3}}{2} a_0^2 \\ &= \frac{\sqrt{3}}{2} (ab + bc + ca) \end{aligned} \quad (\text{B13})$$

where a , b and c are the new edge lengths. Such a deformation consists in an elongation by a factor λ in one direction and by a factor $1/\lambda$ in the perpendicular direction. If we fix the direction of vectors \vec{a}_0 and \vec{a} as on Fig. 4 for convenience, the most general such transformation can be represented by a matrix of the form:

$$F = R_2 \cdot \begin{pmatrix} \lambda & 0 \\ 0 & 1/\lambda \end{pmatrix} \cdot R_1 \quad (\text{B14})$$

where R_1 and R_2 are two rotation matrices.

From Eqs. (B7) to (B9) and (B14), the center-to-center version [13] of the texture tensor [14, 15] can be expressed in matrix form:

$$M = \frac{1}{3} [\vec{u} \cdot \vec{u}^T + \vec{v} \cdot \vec{v}^T + \vec{w} \cdot \vec{w}^T] \quad (\text{B15})$$

$$\begin{aligned} &= \frac{1}{3} R_2 \cdot \begin{pmatrix} \lambda & 0 \\ 0 & 1/\lambda \end{pmatrix} \cdot R_1 \\ &\quad \cdot [\vec{u}_0 \cdot \vec{u}_0^T + \vec{v}_0 \cdot \vec{v}_0^T + \vec{w}_0 \cdot \vec{w}_0^T] \\ &\quad \cdot R_1^{-1} \cdot \begin{pmatrix} \lambda & 0 \\ 0 & 1/\lambda \end{pmatrix} \cdot R_2^{-1} \end{aligned} \quad (\text{B16})$$

$$= \frac{3}{2} a_0^2 R_2 \cdot \begin{pmatrix} \lambda^2 & 0 \\ 0 & 1/\lambda^2 \end{pmatrix} \cdot R_2^{-1} \quad (\text{B17})$$

From Eq. (B17), we obtain:

$$\text{tr}(M) = \frac{3}{2} a_0^2 \left(\lambda^2 + \frac{1}{\lambda^2} \right) \quad (\text{B18})$$

From Eq. (B15) and Eqs. (B10-B12), using the fact that vectors \vec{a} , \vec{b} and \vec{c} meet at angle $2\pi/3$, we obtain another expression for $\text{tr}(M)$:

$$\text{tr}(M) = \frac{1}{6} (L^{\text{dry}})^2 - 3a_0^2 \quad (\text{B19})$$

where $L^{\text{dry}} = 2(a + b + c)$ is the bubble perimeter and where the last term is proportional to the (fixed) bubble surface area $3\sqrt{3}a_0^2/2$, see Eq. (B13).

These two expressions for $\text{tr}(M)$ yield Eq. (B2) for the bubble perimeter L^{dry} in terms of its initial value $L_0^{\text{dry}} = 6a_0$.

The maximum elongation is $\lambda = \sqrt{3}$ for a few, specific orientations of the crystalline network with respect

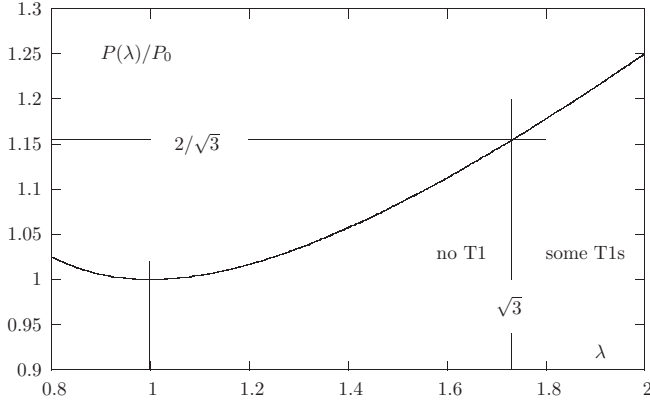


FIG. 5: Bubble perimeter in a crystalline 2D-GG-foam, as a function of elongation λ . The first T1 processes occur when $\lambda = \sqrt{3}$ for specific orientations of the foam. The corresponding bubble perimeter is then about 15% longer than at rest.

to the direction of elongation (it is larger for all other orientations), and this value decreases as the foam becomes wetter as described already long ago [1].

Appendix C: Calculation of the osmotic pressure

In the present paragraph, we will calculate the osmotic pressure of a 2D GG foam. As mentioned in the Introduction, it will later be useful to estimate the foam dilatancy.

When the foam is confined in a container, the osmotic pressure π_{osm} corresponds to the force that must be applied externally to one of the confining walls if the latter is permeable to the liquid but not to the bubbles. The osmotic pressure (which is in fact a symmetric tensor and not just a scalar quantity [6, 7]) is thus the difference between the stress in the foam and the pressure applied by the pure liquid on the other side of the semi-permeable wall:

$$\pi_{\text{osm}} = -p_l - \sigma \quad (\text{C1})$$

(where tensile stresses and pressures are both counted positively). The stress in the foam includes a pressure contribution from the liquid (p_l) and from the gas (p_g), as well as a tensile contribution from the interfaces:

$$\sigma = -\phi p_l I - (1 - \phi) p_g I + \sigma^{\text{interf}}. \quad (\text{C2})$$

Hence,

$$\begin{aligned} \pi_{\text{osm}} &= (1 - \phi) (p_g - p_l) - \sigma^{\text{interf}} \\ &= (1 - \phi) \frac{\gamma}{R_{\text{ps}}} - \sigma^{\text{interf}} \end{aligned} \quad (\text{C3})$$

1. Stress due to the interfaces

Together with the liquid and gas pressures, the interfaces in a foam contribute to the stress in the foam, as

they carry surface tension. In the present appendix, we derive a simple expression for this contribution in the situation of interest.

Each element of interface in the foam, whose normal is oriented along some vector \vec{n} , has a stress contribution that is in the plane perpendicular to \vec{n} , hence it is proportional to $[I - \vec{n} \otimes \vec{n}]$.

In general terms, let us decompose the specific surface area Σ in the foam (surface area per unit volume) according to its orientation:

$$\Sigma = \iint \Sigma(\Omega) \, d\Omega, \quad (\text{C4})$$

where $d\Omega$ represents an element of solid angle. The stress contribution from the interfaces can then be expressed as:

$$\sigma^{\text{interf}} = \gamma \iint [I - \vec{n}(\Omega) \otimes \vec{n}(\Omega)] \Sigma(\Omega) \, d\Omega \quad (\text{C5})$$

where γ is the surface tension.

This implies, in particular, that the orientational average of the interface stress contribution is simply related to the specific surface:

$$\begin{aligned} \langle \sigma^{\text{interf}} \rangle_{3D} &= \frac{1}{3} \text{tr}(\sigma^{\text{interf}}) I \\ &= \frac{2}{3} \gamma \Sigma I \end{aligned} \quad (\text{C6})$$

as already mentioned through Eq. (C17).

We restrict our calculation to the vertical component $\sigma_{zz}^{\text{interf}}$ and to the in-plane averaged component $\sigma_{pl}^{\text{interf}}$ of the interfacial stress.

Consider a surface element dS whose normal \vec{n} makes an angle θ with the vertical direction. If $\theta = 0$, the surface element is horizontal and it contributes γdS towards $\sigma_{pl}^{\text{interf}}$ and zero towards $\sigma_{zz}^{\text{interf}}$. By contrast, if $\theta = \pi/2$, the surface element is vertical and it contributes $\frac{1}{2}\gamma dS$ towards $\sigma_{pl}^{\text{interf}}$ (where the factor 1/2 comes from the in-plane orientation average) and γdS towards $\sigma_{zz}^{\text{interf}}$. More generally, it contributes $\frac{1+\cos^2\theta}{2}\gamma dS$ towards $\sigma_{pl}^{\text{interf}}$ and $\sin^2\theta \gamma dS$ towards $\sigma_{zz}^{\text{interf}}$.

The contribution from the top and the bottom of a bubble to the in-plane component is:

$$\begin{aligned} \frac{2\gamma}{H \mathcal{A}_{\text{tot}}} &\left\{ \mathcal{A}_{\text{tot}} - [2\sqrt{3} R^2 - \pi (R - D_R)^2] \right. \\ &\quad \left. - (L - 2\pi R) R_{\text{ps}} \right\} \end{aligned}$$

Making the approximation $D_R \simeq R_{\text{ps}}$ in the Plateau border region [10] and using $R_{\text{ps}} \ll L$, this becomes:

$$\frac{2\gamma}{H \mathcal{A}_{\text{tot}}} \left\{ \mathcal{A}_{\text{tot}} - (2\sqrt{3} - \pi) R^2 - L R_{\text{ps}} \right\} \quad (\text{C7})$$

The contribution from the vertical films towards $\sigma_{zz}^{\text{interf}}$ is:

$$\frac{\gamma}{H \mathcal{A}_{\text{tot}}} L (H - 2R_{\text{ps}}) \quad (\text{C8})$$

Their contribution to $\sigma_{pl}^{\text{interf}}$ is twice as less due to the orientation average.

The contribution to $\sigma_{zz}^{\text{interf}}$ from the menisci, considered as circular quarter cylinders with radius R_{ps} , can be written as:

$$\frac{\gamma}{H \mathcal{A}_{\text{tot}}} 2L \int_0^{\frac{\pi}{2}} \sin^2 \theta R_{ps} d\theta = \frac{\gamma}{H \mathcal{A}_{\text{tot}}} \frac{\pi}{2} L R_{ps} \quad (\text{C9})$$

Their contribution to $\sigma_{pl}^{\text{interf}}$ is very similar:

$$\begin{aligned} \frac{\gamma}{H \mathcal{A}_{\text{tot}}} 2L \int_0^{\frac{\pi}{2}} \frac{1 + \cos^2 \theta}{2} R_{ps} d\theta \\ = \frac{\gamma}{H \mathcal{A}_{\text{tot}}} \frac{3\pi}{4} L R_{ps} \end{aligned} \quad (\text{C10})$$

The in-plane interface stress component thus includes contributions from Eqs. (C7), (C8) and (C10):

$$\begin{aligned} \frac{H \mathcal{A}_{\text{tot}}}{\gamma} \sigma_{pl}^{\text{interf}} \simeq & 2 \left[\mathcal{A}_{\text{tot}} - (2\sqrt{3} - \pi) R^2 - L R_{ps} \right] \\ & + \frac{1}{2} L (H - 2R_{ps}) \\ & + \frac{3\pi}{4} L R_{ps} \end{aligned} \quad (\text{C11})$$

As for the vertical interface stress component, it includes contributions from Eqs. (C8) and (C9):

$$\begin{aligned} \frac{H \mathcal{A}_{\text{tot}}}{\gamma} \sigma_{zz}^{\text{interf}} \simeq & L (H - 2R_{ps}) \\ & + \frac{\pi}{2} L R_{ps} \end{aligned} \quad (\text{C12})$$

From these two equations, we obtain the final results both in the pancake regime where $R_{ps}^{\text{ABCD}} \simeq \frac{H}{2} [1 - H/(3R)]$ (see Ref. [8]) and where $R_{ps} \ll R$ (regimes A-D of Fig. 3) and in the floor tile regime where $R_{ps} = R$ (E-G):

$$\sigma_{zz}^{\text{interf}} \simeq \frac{\pi}{4} \frac{\gamma L}{\mathcal{A}_{\text{tot}}} + \frac{4 - \pi}{12} \frac{\gamma L H}{\mathcal{A}_{\text{tot}} R} \quad (\text{C13})$$

$$\begin{aligned} \sigma_{pl}^{\text{interf}} \simeq & 2 \frac{\gamma}{H} - (4\sqrt{3} - 2\pi) \frac{\gamma R^2}{\mathcal{A}_{\text{tot}} H} \\ & + \frac{3\pi - 8}{8} \frac{\gamma L}{\mathcal{A}_{\text{tot}}} + \frac{4 - \pi}{8} \frac{\gamma L H}{\mathcal{A}_{\text{tot}} R} \end{aligned} \quad (\text{C14})$$

$$\sigma_{zz}^{\text{interf}} \simeq \frac{\gamma L}{\mathcal{A}_{\text{tot}}} - \frac{4 - \pi}{2} \frac{\gamma L R}{\mathcal{A}_{\text{tot}} H} \quad (\text{C15})$$

$$\begin{aligned} \sigma_{pl}^{\text{interf}} \simeq & 2 \frac{\gamma}{H} + \frac{1}{2} \frac{\gamma L}{\mathcal{A}_{\text{tot}}} - \frac{3(4 - \pi)}{4} \frac{\gamma L R}{\mathcal{A}_{\text{tot}} H} \\ & - (4\sqrt{3} - 2\pi) \frac{\gamma R^2}{\mathcal{A}_{\text{tot}} H} \end{aligned} \quad (\text{C16})$$

Note that as expected from the discussion at the beginning of the present Appendix and as can be checked from the corresponding expressions of the specific surface

area [10], the average of all three components is simply related to the total specific surface area Σ :

$$\frac{2\sigma_{pl}^{\text{interf}} + \sigma_{zz}^{\text{interf}}}{3} = \frac{2}{3} \gamma \Sigma \quad (\text{C17})$$

where the numerical factor 2/3 simply reflects the fact that each surface element contributes tensile stress in two out of three directions of space.

2. Expression of the osmotic pressure

The interfacial contribution σ^{interf} to the stress is calculated in Appendix C1 with the same geometrical approximations as the liquid volume given by Eq. (4). The value is averaged over the sample thickness. For simplicity, we also average in-plane contributions over their orientations. We thus have one value for the vertical component and one value for the in-plane averaged component. The vertical films in the foam contribute plainly to the vertical component and partly (due to the orientation average) to the in-plane component. The interface in the Plateau and pseudo Plateau borders make an angle with the vertical direction: they contribute partly to both components. As for the top and bottom interfaces of the bubbles, they contribute plainly to the in-plane components.

The results from Appendix C1 are as follows:

$$\sigma_{zz}^{\text{interf}} \simeq \frac{\pi}{4} \frac{\gamma L}{\mathcal{A}_{\text{tot}}} + \frac{4 - \pi}{12} \frac{\gamma L H}{\mathcal{A}_{\text{tot}} R} \quad (\text{C18})$$

$$\begin{aligned} \sigma_{pl}^{\text{interf}} \simeq & 2 \frac{\gamma}{H} - (4\sqrt{3} - 2\pi) \frac{\gamma R^2}{\mathcal{A}_{\text{tot}} H} \\ & + \frac{3\pi - 8}{8} \frac{\gamma L}{\mathcal{A}_{\text{tot}}} + \frac{4 - \pi}{8} \frac{\gamma L H}{\mathcal{A}_{\text{tot}} R} \end{aligned} \quad (\text{C19})$$

$$\sigma_{zz}^{\text{interf}} \simeq \frac{\gamma L}{\mathcal{A}_{\text{tot}}} - \frac{4 - \pi}{2} \frac{\gamma L R}{\mathcal{A}_{\text{tot}} H} \quad (\text{C20})$$

$$\begin{aligned} \sigma_{pl}^{\text{interf}} \simeq & 2 \frac{\gamma}{H} + \frac{1}{2} \frac{\gamma L}{\mathcal{A}_{\text{tot}}} - \frac{3(4 - \pi)}{4} \frac{\gamma L R}{\mathcal{A}_{\text{tot}} H} \\ & - (4\sqrt{3} - 2\pi) \frac{\gamma R^2}{\mathcal{A}_{\text{tot}} H} \end{aligned} \quad (\text{C21})$$

In regimes A-D, the first term in Eq. (C3) can be written as:

$$(1 - \phi) \frac{\gamma}{R_{ps}} \simeq (1 - \phi) \left[2 \frac{\gamma}{H} + \frac{2}{3} \frac{\gamma}{R} \right] \quad (\text{C22})$$

In regimes E-G, it reduces to:

$$(1 - \phi) \frac{\gamma}{R_{ps}} \simeq (1 - \phi) \frac{\gamma}{R} \quad (\text{C23})$$

From Eqs. (A3-A4), (C3), (C13-C16) and (C22-C23)

and using $\frac{1}{1-\phi} = \frac{A_{\text{tot}} H}{\Omega}$, we derive the osmotic pressure:

$$\frac{\pi_{\text{osm}}^{zz \text{ ABCD}}}{1-\phi} \simeq 2 \frac{\gamma}{H} + \frac{2}{3} \frac{\gamma}{R} - \frac{\pi}{4} \frac{\gamma L H}{\Omega} \quad (\text{C24})$$

$$\frac{\pi_{\text{osm}}^{pl \text{ ABCD}}}{1-\phi} \simeq \frac{2}{3} \frac{\gamma}{R} - \frac{\pi}{8} \frac{\gamma L H}{\Omega} \quad (\text{C25})$$

$$\frac{\pi_{\text{osm}}^{zz \text{ EFG}}}{1-\phi} \simeq \frac{\gamma}{R} - \frac{\gamma L H}{\Omega} + \frac{4-\pi}{2} \frac{\gamma L R}{\Omega} \quad (\text{C26})$$

$$\frac{\pi_{\text{osm}}^{pl \text{ EFG}}}{1-\phi} \simeq \frac{\gamma}{R} - 2 \frac{\gamma}{H} - \frac{1}{2} \frac{\gamma L H}{\Omega} \quad (\text{C27})$$

Note that in regime E, Eq. (C27) yields the expression $\pi_{\text{osm}}^{pl \text{ D}} \simeq (1-\phi) \left[\frac{\gamma}{R} - \frac{\gamma L H}{2\Omega} \right] - \frac{2\gamma}{H}$ announced earlier [8].

Appendix D: Calculation of the dilatancy and change in volume fraction

1. Remark on the calculations

In the following paragraphs, in order to derive such quantities as the elastic modulus, the dilatancy coefficient or the change in volume fraction upon deformation, we will need to differentiate several equations such as Eqs. (A3-A4) and (C24-C27) and the expressions for the specific surface area [10].

When conducting such calculations, we consider that the gas volume Ω as well as the distance H between the solid plates remain constant.

Once the differentiation is performed, we determine the relative orders of magnitudes of the different terms by using such estimates as:

$$\Omega \propto L^2 H \quad (\text{D1})$$

$$R \ll L \quad (\text{or } \phi \ll 1) \quad (\text{D2})$$

$$H \ll R \quad (\text{ABCD}) \quad (\text{D3})$$

$$R \ll H \quad (\text{EFG}) \quad (\text{D4})$$

$$(\text{D5})$$

and simplify the results accordingly. Performing such simplifications prior to differentiation would erroneously suppress some relevant terms.

We also assimilate the true perimeter L of the bubble and the “dry” perimeter L^{dry} used to derive Eqs. (B2) and (B3). The former is the perimeter of the light grey region in Fig. 2, while the latter is the perimeter that includes the black regions. Because the Plateau border regions (medium grey sector in Fig. 2) correspond to an angle $\pi/3$, they are related through:

$$L^{\text{dry}} - L = (4\sqrt{3} - 2\pi) R \quad (\text{D6})$$

Hence, their relative difference is of order R/L , which is small in all regimes A-G ($\phi \ll 1$).

2. Change in the Plateau border radius

The foam deformation, which generates an increase in the bubble perimeter given by Eq. (B3), causes a change in the radius of curvature of the Plateau borders.

From Eq. (A3):

$$\frac{\delta\phi^{\text{ABCD}}}{(1-\phi^{\text{ABCD}})^2} \simeq \frac{4-\pi}{8} \frac{H^2}{\Omega} \delta L + \left[(4\sqrt{3} - 2\pi) \frac{R H}{\Omega} + \frac{4-\pi}{12} \frac{H^3 L}{\Omega R^2} \right] \delta R \quad (\text{D7})$$

Hence, with $\delta\phi^{\text{ABCD}} = 0$ and $\phi^{\text{ABCD}} \ll 1$:

$$\delta R^{\text{ABCD}}|_{\delta\phi=0} \simeq \frac{-\frac{3}{2} \frac{R^2}{L H}}{1 + \frac{12(4\sqrt{3}-2\pi)}{4-\pi} \frac{R^3}{L H^2}} \delta L \quad (\text{D8})$$

From Eq. (A4):

$$\frac{\delta\phi^{\text{EFG}}}{(1-\phi^{\text{EFG}})^2} \simeq \frac{4-\pi}{2} \frac{R^2}{\Omega} \delta L + \left[(4-\pi) \frac{R L}{\Omega} + (4\sqrt{3} - 2\pi) \frac{R H}{\Omega} \right] \delta R \quad (\text{D9})$$

Hence, with $\delta\phi^{\text{EFG}} = 0$ and $\phi^{\text{EFG}} \ll 1$:

$$\delta R^{\text{EFG}}|_{\delta\phi=0} \simeq \frac{-\frac{1}{2} \frac{R}{L}}{1 + \frac{4\sqrt{3}-2\pi}{4-\pi} \frac{H}{L}} \delta L \quad (\text{D10})$$

The results of Eqs. (D8) and (D10) above are reported in Table III.

3. Shear modulus

The average bubble surface area, and hence the foam interfacial energy, also change as a consequence of the increase in the bubble perimeter given by Eq. (B3). When taken at constant liquid fraction ϕ (or equivalently at constant A_{tot}), this change is directly related to the shear modulus of the foam. From the expressions of the specific surface area obtained in Ref. [10], we obtain:

$$\frac{\delta\Sigma^{\text{ABCD}}|_{\phi}}{1-\phi} \simeq - \left[(8\sqrt{3} - 4\pi) \frac{R}{\Omega} + \frac{4-\pi}{6} \frac{L H^2}{\Omega R^2} \right] \delta R + \left[\frac{\pi-2}{2} \frac{H}{\Omega} + \frac{4-\pi}{6} \frac{H^2}{\Omega R} \right] \delta L \quad (\text{D11})$$

$$\frac{\delta\Sigma^{\text{EFG}}|_{\phi}}{1-\phi} \simeq - \left[(4-\pi) \frac{L}{\Omega} + (8\sqrt{3} - 4\pi) \frac{R}{\Omega} \right] \delta R + \left[\frac{H}{\Omega} - (4-\pi) \frac{R}{\Omega} \right] \delta L \quad (\text{D12})$$

These equations, taken at constant volume fraction ($\delta\phi = 0$) and with $\phi \ll 1$, together with Eqs. (D8)

and (D10), yield:

$$\frac{\delta\Sigma_{ABCD}|_\phi}{\delta L/L} \simeq \frac{\pi}{4} \frac{L H}{\Omega} \quad (\text{D13})$$

$$\frac{\delta\Sigma_{EFG}|_\phi}{\delta L/L} \simeq \frac{L H}{\Omega} \quad (\text{D14})$$

where it turns out that Eq. (D14) for regimes E-G results just from the change in perimeter, *i.e.*, the δL term in Eq. (D12). By contrast, for regimes A-D, the result of Eq. (D13) depends partly on the reduction in Plateau border radius (δR term) in Eq. (D11) caused by the deformation.

Let us now derive the shear modulus G from the above equations. In the case of a foam, the elastic energy per unit volume in the material is given by the change in specific surface area caused by some (small) shear strain Γ , multiplied by surface tension:

$$\frac{1}{2} G \Gamma^2 = \gamma \delta\Sigma(\Gamma) \quad (\text{D15})$$

Now, because shear causes both deformation and rotation, the effect of a strain Γ on elongation is halved: $\lambda = 1 + \Gamma/2$. Hence, Eq. (B3) yields:

$$\left. \frac{\delta L}{L} \right|_\phi \simeq \frac{\Gamma^2}{8} \quad (\text{D16})$$

Using Eqs. (D15) and (D16), the shear modulus in the pancake and in the floor tile regimes can now be derived from Eqs. (D13) and (D14):

$$G^{ABCD} \simeq \frac{\pi}{16} \frac{\gamma L H}{\Omega} \quad (\text{D17})$$

$$G^{EFG} \simeq \frac{1}{4} \frac{\gamma L H}{\Omega} \quad (\text{D18})$$

The results of Eqs. (D17) and (D18) above are reported in Table II.

4. Change in osmotic pressure

The change in bubble perimeter also causes a change in osmotic pressure.

From Eqs. (C24-C27), we obtain:

$$\begin{aligned} \frac{\delta\pi_{\text{osm}}^{zz\text{ ABCD}}}{1-\phi} + \frac{\pi_{\text{osm}}^{zz\text{ ABCD}} \delta\phi}{(1-\phi)^2} \\ \simeq -\frac{2}{3} \frac{\gamma}{R^2} \delta R - \frac{\pi}{4} \frac{\gamma H}{\Omega} \delta L \end{aligned} \quad (\text{D19})$$

$$\begin{aligned} \frac{\delta\pi_{\text{osm}}^{pl\text{ ABCD}}}{1-\phi} + \frac{\pi_{\text{osm}}^{pl\text{ ABCD}} \delta\phi}{(1-\phi)^2} \\ \simeq -\frac{2}{3} \frac{\gamma}{R^2} \delta R - \frac{\pi}{8} \frac{\gamma H}{\Omega} \delta L \end{aligned} \quad (\text{D20})$$

$$\begin{aligned} \frac{\delta\pi_{\text{osm}}^{zz\text{ EFG}}}{1-\phi} + \frac{\pi_{\text{osm}}^{zz\text{ EFG}} \delta\phi}{(1-\phi)^2} \\ \simeq -\frac{\gamma}{R^2} \delta R - \frac{\gamma H}{\Omega} \delta L \end{aligned} \quad (\text{D21})$$

$$\begin{aligned} \frac{\delta\pi_{\text{osm}}^{pl\text{ EFG}}}{1-\phi} + \frac{\pi_{\text{osm}}^{pl\text{ EFG}} \delta\phi}{(1-\phi)^2} \\ \simeq -\frac{\gamma}{R^2} \delta R - \frac{\gamma H}{2\Omega} \delta L \end{aligned} \quad (\text{D22})$$

where some terms have been neglected as explained in Paragraph D 1.

At constant volume fraction ($\delta\phi = 0$) and with $\phi \ll 1$, the above equations now yield, using Eqs. (D8) and (D10):

$$\frac{\delta\pi_{\text{osm}}^{zz\text{ ABCD}}}{\delta L/L} \simeq \frac{\frac{\gamma}{H} - \frac{3\pi(4\sqrt{3}-2\pi)}{(4-\pi)} \frac{\gamma R^3}{\Omega H}}{1 + \frac{12(4\sqrt{3}-2\pi)}{4-\pi} \frac{R^3}{H^2 L}} \quad (\text{D23})$$

$$\frac{\delta\pi_{\text{osm}}^{pl\text{ ABCD}}}{\delta L/L} \simeq \frac{\frac{\gamma}{H} - \frac{3\pi(4\sqrt{3}-2\pi)}{2(4-\pi)} \frac{\gamma R^3}{\Omega H}}{1 + \frac{12(4\sqrt{3}-2\pi)}{4-\pi} \frac{R^3}{H^2 L}} \quad (\text{D24})$$

$$\frac{\delta\pi_{\text{osm}}^{zz\text{ EFG}}}{\delta L/L} \simeq -\frac{\gamma H L}{\Omega} + \frac{\frac{\gamma}{2R}}{1 + \frac{4\sqrt{3}-2\pi}{4-\pi} \frac{H}{L}} \quad (\text{D25})$$

$$\frac{\delta\pi_{\text{osm}}^{pl\text{ EFG}}}{\delta L/L} \simeq -\frac{\gamma H L}{2\Omega} + \frac{\frac{\gamma}{2R}}{1 + \frac{4\sqrt{3}-2\pi}{4-\pi} \frac{H}{L}} \quad (\text{D26})$$

where, again, some terms have been neglected. These results are reported in Table III in each asymptotic regime, using the relations of Table I. Note that both normal and in-plane dilatancy are negative not only in regime G as mentioned in ref. [8], but also in regime A.

5. Elastic dilatancy in GG foams: shear or elongation, in-plane or normal

There are of course two versions of dilatancy, depending on whether the osmotic pressure is measured in the plane of deformation or in the normal direction. But the value of the coefficient defined by Eq. (1) depends on the deformation mode that is considered. Hence, for an elongation by a factor $\lambda = 1 + \epsilon$ or for a shear strain Γ , the variation of the osmotic pressure and the definition of the

dilatancy coefficient will be:

$$\pi_{\text{osm}} \simeq \pi_{\text{osm}}^0 + \frac{\epsilon^2}{2} \frac{\partial^2 \pi_{\text{osm}}}{\partial \epsilon^2} \Big|_{\phi} \quad \chi^{\text{el}} = \frac{\partial^2 \pi_{\text{osm}}}{\partial \epsilon^2} \Big|_{\phi} \quad (\text{D27})$$

$$\pi_{\text{osm}} \simeq \pi_{\text{osm}}^0 + \frac{\Gamma^2}{2} \frac{\partial^2 \pi_{\text{osm}}}{\partial \Gamma^2} \Big|_{\phi} \quad \chi^{\text{sh}} = \frac{\partial^2 \pi_{\text{osm}}}{\partial \Gamma^2} \Big|_{\phi} \quad (\text{D28})$$

The dilatancy coefficient can thus be expressed as:

$$\chi^{\text{el}} = \frac{\delta \pi_{\text{osm}}(\epsilon)|_{\phi}}{\epsilon^2/2} \quad (\text{D29})$$

$$\chi^{\text{sh}} = \frac{\delta \pi_{\text{osm}}(\Gamma)|_{\phi}}{\Gamma^2/2} \quad (\text{D30})$$

Now, for elongation, the usual definition of a deformation ϵ is that the material is elongated by a factor $\lambda = 1 + \epsilon$. Hence, Eq. (B3) yields:

$$\frac{\delta L}{L} \Big|_{\phi} \simeq \frac{\epsilon^2}{2} \quad (\text{D31})$$

As a result of Eqs. (D16) and (D31), the dilatancy coefficients for elongation and shear deformation modes can be expressed as:

$$\chi^{\text{el}} \simeq \frac{\delta \pi_{\text{osm}}|_{\phi}}{(\delta L/L)|_{\phi}} \quad (\text{D32})$$

$$\chi^{\text{sh}} = \frac{1}{4} \chi^{\text{el}} \quad (\text{D33})$$

From Eq. (D32) and Eqs. (D23-D26), the elongation normal and in-plane dilatancies are indicated in Table III for each regime specified in Table I.

6. Change in volume fraction

We shall now calculate the change in liquid volume fraction ϕ that results from the foam deformation (change

in perimeter) under constant (normal or in-plane) osmotic pressure.

To do this, we set $\delta \pi_{\text{osm}} = 0$ in Eqs. (D19-D22) and we eliminate δR between each of these equations and Eq. (D7) or (D9). We thus obtain:

$$\frac{\delta \phi^{\text{ABCD}}}{\delta L/L} \Big|_{\pi_{\text{osm}}^{zz}} \simeq \frac{\frac{4-\pi}{8} \frac{H^2 L}{\Omega} - \frac{3\pi(4\sqrt{3}-2\pi)}{8} \frac{R^3 H^2 L}{\Omega^2}}{1 + 3(4\sqrt{3}-2\pi) \frac{R^3}{\Omega}} \quad (\text{D34})$$

$$\frac{\delta \phi^{\text{ABCD}}}{\delta L/L} \Big|_{\pi_{\text{osm}}^{pl}} \simeq \frac{4-\pi}{8} \frac{H^2 L}{\Omega} - \frac{3\pi(4\sqrt{3}-2\pi)}{16} \frac{R^3 H^2 L}{\Omega^2} \quad (\text{D35})$$

$$\frac{\delta \phi^{\text{EFG}}}{\delta L/L} \Big|_{\pi_{\text{osm}}^{zz}} \simeq \frac{4-\pi}{2} \frac{R^2 L}{\Omega} - (4\sqrt{3}-2\pi) \frac{R^3 H^2 L}{\Omega^2} \quad (\text{D36})$$

$$\frac{\delta \phi^{\text{EFG}}}{\delta L/L} \Big|_{\pi_{\text{osm}}^{pl}} \simeq \frac{4-\pi}{2} \frac{R^2 L}{\Omega} - (2\sqrt{3}-\pi) \frac{R^3 H^2 L}{\Omega^2} \quad (\text{D37})$$

The relative change in liquid volume fraction can then be obtained from Eqs. (A3-A4):

$$\frac{\delta \phi/\phi}{\delta L/L} \Big|_{\pi_{\text{osm}}^{zz}}^{\text{ABCD}} \simeq \frac{1 - \frac{3\pi(4\sqrt{3}-2\pi)}{4-\pi} \frac{R^3}{\Omega}}{\left[1 + 3(4\sqrt{3}-2\pi) \frac{R^3}{\Omega}\right] \left[1 + \frac{4(4\sqrt{3}-2\pi)}{4-\pi} \frac{R^2}{LH}\right]} \quad (\text{D38})$$

$$\frac{\delta \phi/\phi}{\delta L/L} \Big|_{\pi_{\text{osm}}^{pl}}^{\text{ABCD}} \simeq \frac{1 - \frac{3\pi(4\sqrt{3}-2\pi)}{2(4-\pi)} \frac{R^3}{\Omega}}{1 + \frac{4(4\sqrt{3}-2\pi)}{4-\pi} \frac{R^2}{LH}} \quad (\text{D39})$$

$$\frac{\delta \phi/\phi}{\delta L/L} \Big|_{\pi_{\text{osm}}^{zz}}^{\text{EFG}} \simeq \frac{1 - \frac{2(4\sqrt{3}-2\pi)}{4-\pi} \frac{R H^2}{\Omega}}{1 + \frac{4\sqrt{3}-2\pi}{4-\pi} \frac{H}{L}} \quad (\text{D40})$$

$$\frac{\delta \phi/\phi}{\delta L/L} \Big|_{\pi_{\text{osm}}^{pl}}^{\text{EFG}} \simeq \frac{1 - \frac{4\sqrt{3}-2\pi}{4-\pi} \frac{R H^2}{\Omega}}{1 + \frac{4\sqrt{3}-2\pi}{4-\pi} \frac{H}{L}} \quad (\text{D41})$$

-
- [1] D. Weaire and S. Hutzler, *The Physics of Foams* (Oxford University Press, 1999).
 - [2] I. Cantat, S. Cohen-Addad, F. Elias, F. Graner, R. H. "ohler, O. Pitois, F. Rouyer, and A. Saint-Jalmes, *Les mousses - structure et dynamique* (Belin, Paris, 2010).
 - [3] O. Reynolds, *Philos. Mag.* **20**, 469 (1985).
 - [4] R. Bagnold, *The physics of blown sand and desert dunes* (Chapman and Hall, London, 1941).
 - [5] S. Marze, A. Saint-Jalmes, and D. Langevin, *Colloids and Surface A* **263**, 121 (2005).
 - [6] D. Weaire and S. Hutzler, *Phil. Mag.* **83**, 2747 (2003).
 - [7] F. Rioual, S. Hutzler, and D. Weaire, *Coll. Surf. A* **263**, 117 (2005).
 - [8] P. Rognon, F. Molino, and C. Gay, *EPL (Europhysics Letters)* **90**, 38001 (2010).
 - [9] M. Vaz and S. Cox, *Philosophical Magazine Letters* **85**, 415 (2005).
 - [10] P. Rognon, C. Gay, D. Reinelt, and F. Molino, *subm. to Eur. Phys. J. E* (2010), <http://hal.archives-ouvertes.fr/hal-00361004/fr/>.
 - [11] S. Cox, D. Weaire, and M. Vaz, *The European Physical Journal E: Soft Matter and Biological Physics* **7**, 311 (2002), ISSN 1292-8941, URL <http://dx.doi.org/10.1140/epje/i2001-10099-1>.
 - [12] S. Cox and E. Janiaud, *Philosophical Magazine Letters* **88**, 693 (2008).
 - [13] F. Graner, B. Dollet, C. Raufaste, and P. Marmottant, *Eur. Phys. J. E* **25**, 349 (2008), arXiv:0708.3193 [cond-mat.soft].
 - [14] M. Aubouy, Y. Jiang, J. Glazier, and F. Graner, *Granular Matter* **5**, 67 (2003).
 - [15] M. Asipauskas, M. Aubouy, J. Glazier, F. Graner, and

Y. Jiang, Granular Matter **5**, 71 (2003).

- [16] Surprisingly, the increase in bubble perimeter does not depend on the crystal orientation with respect to the di-

rection of elongation.